DETERMINATION OF THE FABRIC ALTERATION OF MARINE CLAYS

SUCHIT D. GUMASTE, KANNAN R. IYER, SUSMITA SHARMA and D.N. SINGH

about the authors

Suchit D. Gumaste
Indian Institute of Technology Bombay,
Department of Civil Engineering
Powai, Mumbai-400076, India
E-mail: suchit.gumaste@gmail.com

Kannan R. Iyer
Indian Institute of Technology Bombay,
Department of Civil Engineering
Powai, Mumbai-400076, India
E-mail: kannankr20@gmail.com

Susmita Sharma
Indian Institute of Technology Bombay,
Department of Civil Engineering
Powai, Mumbai-400076, India
E-mail: susmita.sharma4@gmail.com

corresponding author

Devendra Narain Singh
Indian Institute of Technology Bombay,
Department of Civil Engineering
Powai, Mumbai-400076, India
E-mail: dns@civil.iitb.ac.in

Abstract

This paper presents details of investigations that were conducted to determine the fabric (i.e., the arrangement of soil grains and pores) of undisturbed marine clay samples that were retrieved from 5 m to 65 m below the seabed. Impedance Spectroscopy (IS), which is a non-destructive and non-invasive technique, was employed to determine the electrical conductivities of the marine clay samples in their longitudinal and transverse planes of sedimentation. These results were employed to define the extent of the fabric anisotropy in terms of an anisotropy coefficient, A_e, as a function of depth. In addition, Scanning Electron Microscopy (SEM) and Mercury Intrusion Porosimetry (MIP) were employed to study the fabric and pore-size distribution of these samples, respectively. Based on these investigations it has been observed that A_e increases with sampling depth, which is indicative of the alteration from flocculated fabric, at shallower depths, to the dispersed fabric, at deeper depths. The study highlights the importance and usefulness of the anisotropy coefficient, A_e, for determining the alteration in the fabric of marine clays, due to self-weight consolidation.

keywords

Marine clays, anisotropy, laboratory tests

NOTATIONS

σ_{dc}	DC conductivity of the sample
η	porosity of the sample
G	specific gravity
e	voids ratio
γ_d,γ_t	dry and total unit weight of the sample, respectively
w	gravimetric water content
ω	frequency of the AC
σ_{dct}, σ_{dcl}	DC conductivity in the transverse and longitudinal directions, respectively
σ_{AC}	AC conductivity
A	area of the electrodes
A_e	anisotropy coefficient
d_s	sampling depth
d	pore diameter
d_m	mean pore diameter
d_d	dominant pore diameter
IS	impedance spectroscopy
l	distance between the electrodes
L/S	liquid to solid
MIP	mercury intrusion porosimetry
P	pressure
SEM	scanning electron microscopy
V_{Hg}	cumulative volume of mercury intruded in the sample
V_{HgI}	incremental volume of mercury intruded in the sample
Z'	real part of the impedance

1 INTRODUCTION

Marine clays are formed through a process of the sedimentation of suspended particles in seawater. During this process, clay and silt particles flocculate and settle as flocs on the seabed due to the cations present in the seawater [1]. When more and more flocs accumulate at the top, the bottom layers consolidate due to the weight of the sediments lying above. This process, called self-weight consolidation, was previously studied by other researchers [2-6]. Marine clays are soft in consistency and hence exhibit a poor shear strength and a high compressibility [7], and hence due to such adverse engineering behaviour, these soils pose great challenges to the civil-engineering profession [8].

An overview of the studies conducted by previous researchers [9-18] reveals that factors like degree of consolidation, extent of agglomeration, swelling and shrinkage characteristics of sediments, and the chemical constituents of seawater, are responsible for the post-sedimentation fabric (i.e., the spatial arrangement of the particles and the pores) of marine clays. Therefore, a close interrelation between the fabric, and the origin and degree of consolidation of marine clays is expected. Also, as soil fabric is one of the major factors influencing the strength and deformation characteristics of clays [17, 19-34], investigations into the fabric of marine clays that have undergone varying degrees of self-weight consolidation need to be conducted.

In this context, efforts made by some of the previous researchers are worth mentioning. The fabric of marine clays, corresponding to the same depths below the seabed, from the eastern and western coastal cities of India, has been studied with the help of Scanning Electron Microscopy (SEM) [17], and it has been reported that these soils exhibit a mainly flocculated or dispersed fabric, depending upon the characteristics of the depositional environment (e.g., the chemical constituents of seawater). Incidentally, researchers [35] have proposed various models to explain the flocculated, random and dispersed fabric. Efforts have also been made by researchers [36, 37] to study the interrelation between the microstructure of clays and their physical properties using the XRD and SEM techniques. In this context, the mineralogical and micro-fabric analyses of marine clays from Hong Kong are worth mentioning [38, 39].

However, not many efforts have been made to establish a correlation between the fabric of the marine clays with the conditions prevailing during their formation and the degree of compactness, in a quantitative manner. It is believed that such relations would be helpful in understanding the overall effect of the process of self-weight consolidation on the fabric changes in these clays. It should be noted that changes in the fabric also influence the degree of anisotropy of the permeability, shear strength, and other physical properties, as reported by previous researchers [40], and hence quantification of the fabric changes in terms of the fabric anisotropy becomes essential.

Keeping in view the above-mentioned aspects, investigations were carried out on undisturbed marine clays, retrieved from different depths below the seabed. The main objective of these investigations is to quantify the change in the fabric anisotropy with respect to the sampling depth and thereby to elaborate how the fabric of marine clays alters when they are subjected to self-weight consolidation. Details of the investigations performed to achieve this objective are presented in the following.

2 LABORATORY INVESTIGATIONS

2.1 DETAILS OF THE SAMPLES

Undisturbed marine clay samples (Table 1), collected from the south-eastern coast of India, were used in this study. These samples were retrieved from the same borehole with the help of Shelby tubes of internal diameter 76mm, pushed from the seabed and then transferred to PVC tubes (200 mm long, 90 mm internal diameter and 2 mm wall thickness). Due care was taken to prevent the migration of moisture from the sample, and any physical damage occurring to it, during its transportation from the site to the laboratory, by wrapping it with a cellophane membrane and a bubbled polythene sheet. Both sides of these tubes were covered with PVC caps and sealed with wax. The depth of these samples ranged from 5 to 65 m below the seabed. The specific gravity G of these samples was determined with the help of a helium gas pycnometer (Quantachrome, USA) [41,42]. The total unit weight γ_t, water content w, dry density γ_d, voids ratio e, and porosity η, of these samples were also determined (Table 1).

2.2 PHYSICAL CHARACTERIZATION

A certain portion of each sample was oven dried at 105±5 °C, pulverized, and used for establishing the particle size distribution characteristics [43] and the consistency limits [44]. The results obtained from this exercise are presented in Table 2. Based on the Unified Soil Classification System (USCS) [45] classification, as

Table 1. Physical properties of the samples.

Sample designation	Depth (m)	water content, w (%)	Total unit weight, γ_t (kN/m^3)	Dry unit weight, γ_d (kN/m^3)	Specific gravity, G	void ratio, e	Porosity, η (%)
S1	5.50	50.6	16.8	11.2	2.56	1.29	56
S2	8.45	35.7	17.9	13.2	2.73	1.07	52
S3	9.45	38.2	20.5	14.8	2.91	0.96	49
S4	12.50	56.0	18.9	12.1	2.51	1.07	52
S5	15.10	27.6	19.0	14.9	2.64	0.77	44
S6	18.55	35.3	19.9	14.7	2.68	0.82	45
S7	21.50	47.6	19.8	13.4	2.48	0.85	46
S8	27.15	32.2	19.7	14.9	2.77	0.86	46
S9	33.50	36.7	19.1	14.0	2.53	0.81	45
S10	36.45	36.9	22.6	16.5	2.73	0.65	40
S11	38.55	28.3	20.6	16.1	2.67	0.66	40
S12	40.55	25.8	21.2	16.9	2.82	0.67	40
S13	47.50	29.4	20.9	16.2	2.49	0.54	35
S14	50.60	56.0	25.5	16.3	2.57	0.57	36
S15	64.40	17.6	21.5	18.3	2.68	0.47	32

Table 2. Physical properties of the samples: Particle size distribution characteristics and classification of the samples.

Sample designation	%			Liquid limit (%)	Plastic limit (%)	Plasticity Index (%)	USCS*
	Clay fraction	Silt fraction	Sand fraction				
S1	60	39	1	65	27	38	MH
S2	53	43	4	71	29	42	CH
S3	66	30	4	72	36	36	MH
S4	54	44	1	73	32	41	CH
S5	57	40	3	78	40	38	MH
S6	60	39	1	77	39	38	MH
S7	59	40	1	78	31	47	CH
S8	64	30	6	80	34	46	CH
S9	65	34	1	78	33	45	CH
S10	63	37	0	72	31	41	CH
S11	60	38	2	78	39	39	MH
S12	59	40	1	76	33	43	CH
S13	78	20	2	82	34	48	CH
S14	73	27	0	97	37	60	CH
S15	62	34	4	78	31	47	CH

* Unified soil classification system (as per ASTM D 2487-06e1)

depicted in Fig. 1, it can be inferred that these samples belong to the MH and CH groups. This indicates that the marine sediments are relatively uniform up to the depth of interest.

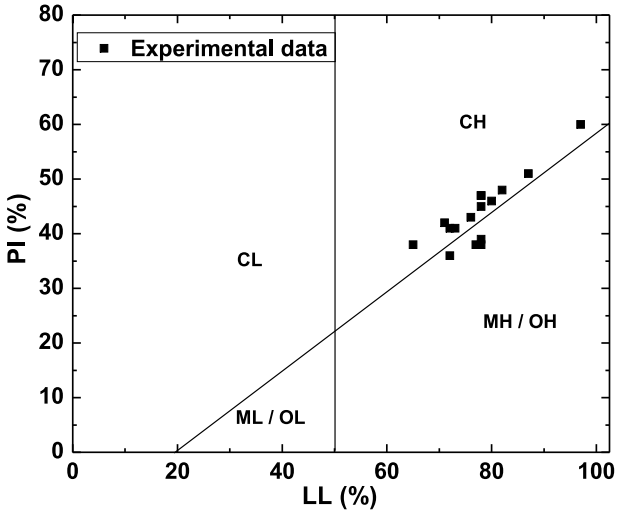

Figure 1. Location of different samples on the USCS plasticity chart.

2.3 CHEMICAL CHARACTERIZATION

The range of chemical composition (by % weight) of the sample, in the form of major oxides, was determined by using an X-ray Fluorescence setup (Phillips 1410, Netherlands). It was observed that these samples contain SiO_2 as a major oxide (58 to 66 %) along with 14 to 17 % of Al_2O_3 and 2 to 13 % of Fe_2O_3.

The chloride and sulphate contents of the sample were determined on an extract of 2:1 water-to-soil ratio (designated as L/S, by weight), with the help of an Indion Easy test kit (supplied by Ion Exchange India Ltd., Mumbai, India). It was observed that these samples have a sulphate content varying between 5 to 30 ppm for an L/S equal to 10 and 20. However, the chloride content of these soils was found to vary from 700 to 1000 ppm and 300 to 550 ppm, for an L/S equal to 10 and 20, respectively. A water-quality analyser (Model PE 136, Elico Ltd., India), fitted with a glass calomel electrode, was employed for measuring the pH of the soil solution with different liquid-to-solid ratios (L/S=10 and 20). The pH values of these soil solutions fall in the range 8.1 to 8.9.

2.4 INVESTIGATIONS ON THE FABRIC ANISOTROPY

In order to establish the variation of the fabric with the depth of the sampling of the specimen, the anisotropy coefficient, A_e, which is defined by Eq. 1 [46-48], was employed:

$$A_e = \sqrt{\frac{\sigma_{dct}}{\sigma_{dcl}}} \qquad (1)$$

where σ_{dct} and σ_{dcl} are the DC conductivities in the horizontal (i.e., transverse to the plane of sedimentation) and vertical (i.e., longitudinal to the plane of sedimentation) directions, respectively.

The methodology based on Impedance Spectroscopy (IS) [49-51], developed by previous researchers [48], was employed to measure σ_{dct} and σ_{dcl} and hence to compute A_e. In addition, Scanning Electron Microscopy (SEM) and Mercury Intrusion Porosimetry (MIP) were also conducted on the specimens of the samples in order to observe the particle-to-particle interaction and the pore size distribution, respectively, as discussed in the following.

2.5 ELECTRICAL CONDUCTIVITY MEASUREMENTS

With the help of a stainless-steel sample extruder (exhibiting an area ratio of less than 10%) and a piston attached to it, samples (38 mm diameter and 30 mm long) were retrieved from the PVC tubes. To avoid any distortion during the sample collection and extraction, the extruder was lubricated with silicon grease. The DC conductivities, σ_{dc}, of these samples were determined for the longitudinal direction and the transverse direction by employing an LCR (Inductance, Capacitance and Resistance) meter (Agilent 4284A). The methodology for sample preparation, the detailed information regarding the test setup, the method of calibration and the procedure adopted for determining σ_{dc}, reported by previous researchers [48, 52], are discussed in the following.

The test setup, depicted in Fig. 2, was employed for measuring the electrical conductivity, σ_{dc}, of the sample. This setup consists of two acrylic plates (100 mm × 100 mm × 10 mm) and at the centre of each of these plates a stainless-steel electrode (50 mm × 50 mm × 2 mm) is fitted. These electrodes are mirror finished, passivated and are connected to brass bolts, across which an electrical potential can be applied. The sample can be fitted between these plates by adjusting their distance with the help of a steel rod and screws arrangement, as depicted in Fig. 2(d). The calibration of the test setup was made by applying open- and short-circuit corrections, which help in eliminating the unwanted impedance generated due to connecting the cables of the LCR meter and the stray capacitance [48, 52]. After the calibration of the test setup, the σ_{dc} of the sample (38 mm in diameter and 30 mm in height) was determined, as explained in the

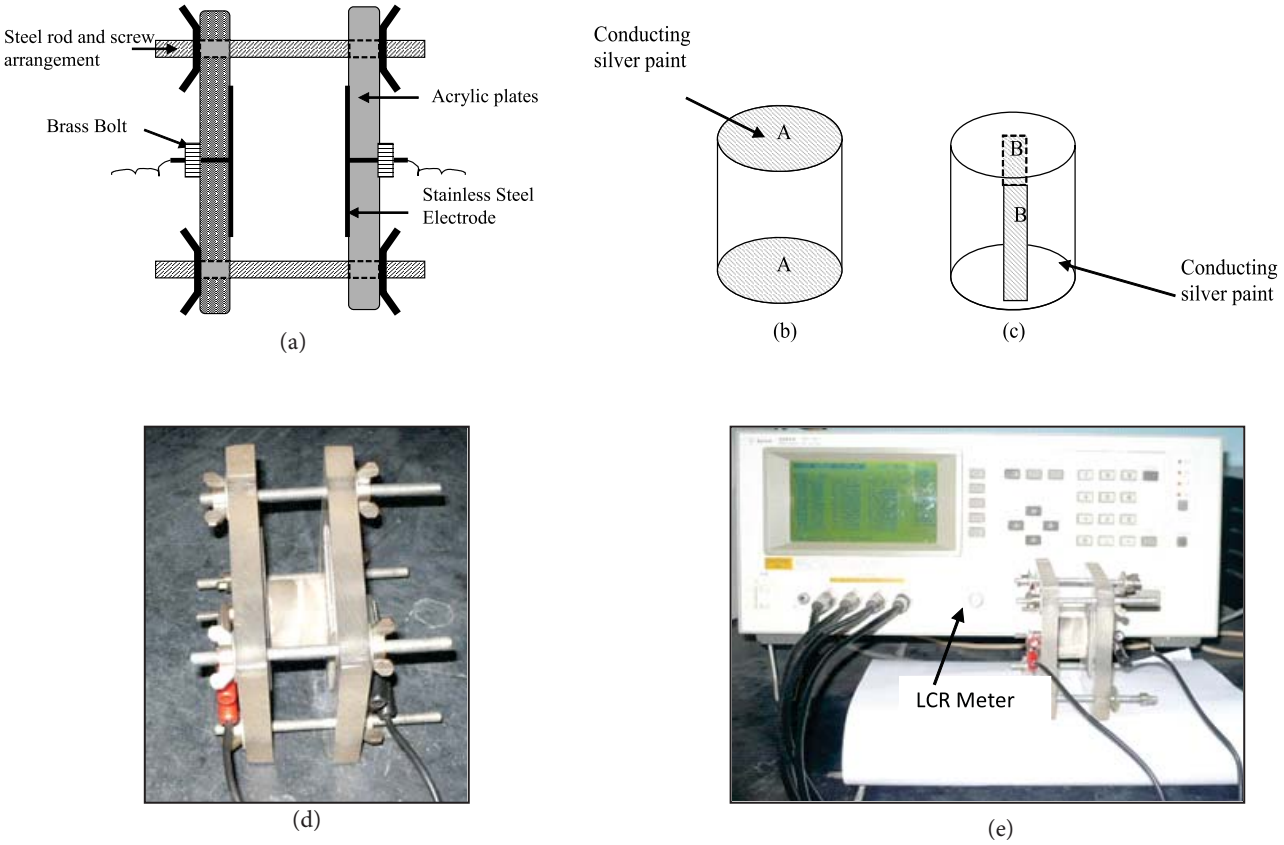

Figure 2. (a) Schematic of the sample holder, (b) Longitudinal (A-A) view of the sample, (c) transverse (B-B) view of the sample, the photographs of (d) the sample holder and (e) the test setup.

following. As depicted in Fig. 2(b and c), the top and bottom surfaces, and the about 10-mm-thick curved surface on the opposite sides of the sample, were painted with a conducting silver paint. Next, the AC conductivity, σ_{AC}, of the sample was determined by employing a LCR meter, which works in the frequency range 20 Hz to 1 MHz and by applying an electric field of 1 V. As reported by previous researchers [52], the real part of the impedance, Z', which gets displayed on the LCR meter corresponding to a different frequency of AC (designated as ω), was recorded and by employing Eq. 2 the σ_{AC} was computed.

$$\sigma_{AC} = \frac{\boldsymbol{l}}{Z' \cdot \boldsymbol{A}} \qquad (2)$$

where $\boldsymbol{l}$ and $\boldsymbol{A}$ are the distance between the electrode plates and area of the electrodes, respectively.

Subsequently, σ_{AC} was plotted with respect to ω (on x-axis) and the intersection of the linear portion of the plot on the σ_{AC} axis (ω=0) was determined, which yields the σ_{dc} of the sample [52].

2.6 DETERMINATION OF SOIL FABRIC

The fabric of the sample was determined using SEM and MIP. To achieve this, approximately 5-mm-sized cubic specimens were extruded from the middle one-third portion of the samples, after the electrical conductivity was recorded. The pore-fluid present in the specimen was removed by employing an air-drying technique [48]. As the soil specimens are non-conducting in nature, there will be a charge accumulation on their surface, which results in blurring and poor quality of the images during the SEM studies. In order to minimize this, the specimens were placed on a sample holder, with a conducting carbon base, and were coated with an about 15-nm-thick gold-palladium (a conducting material) layer by employing a coating device (JCF 1600, JEOL). The SEM images (corresponding to 500× to 8000× magnification and depicting the view perpendicular to the plane of deposition) of the specimen were obtained by employing Quanta 200 ESEM instrument. Although the ESEM allows different modes (i.e., the high-vacuum mode and the ESEM mode) for image capturing, which

also facilitates an analysis of wet specimens, the high-vacuum mode, which necessitates the use of air-dry specimens, was employed in the present study to obtain a better resolution of the images. At lower magnifications, general fabric features were studied, while at higher magnifications the particle assemblage, the type of the contacts and the pore space morphology were inspected.

The pore-size distribution characteristics of the specimen were obtained with the help of a MIP (Quantachrome, USA). The MIP works on the principle that the applied pressure required for the intruding mercury (a non-wetting liquid) into the pores is inversely proportional to their size [53]. The test is performed by increasing the pressure, P (up to 225 MPa, which corresponds to the pore diameter, 0.0064 μm), on the mercury filling the cell containing the sample. The pore-size obtained from the measured pressure, by assuming a contact angle and a surface tension of the mercury as 140° and 0.480 N/m, respectively [54], when plotted against the cumulative volume of the mercury intruded into the sample, V_{Hg}, facilitates a determination of the pore-size distribution characteristics of different specimens (see Fig. 9).

3 RESULTS AND DISCUSSION

The magnitude of σ_{dc} for the soil samples measured in two directions, designated as σ_{dct} and σ_{dcl}, is presented in Table 3. It is clear from the data presented in the table that σ_{dct} is higher than σ_{dcl} for all the samples. This indicates that the electrical conductivity measurements are dependent on the direction along which they are measured and this directional dependency (i.e., electrical anisotropy) can be quantified by employing Eq. 1. Although σ_{dc} depends strongly upon the voids ratio, particle arrangement and the pore-fluid conductivity, A_e would be a function of the anisotropy of the particle arrangement or the fabric anisotropy [48, 55]. With

Table 3. DC Conductivities and anisotropy coefficient of different samples.

Sample designation	Depth (m)	σ_{dcl} (S/m)	σ_{dct} (S/m)	A_e
S1	5.50	2.14	5.53	1.61
S2	8.45	2.84	8.65	1.75
S3	9.45	2.86	9.06	1.78
S4	12.50	2.52	6.92	1.66
S5	15.10	3.10	9.40	1.74
S6	18.55	2.79	9.14	1.81
S7	21.50	1.95	6.53	1.82
S8	27.15	2.34	9.13	1.97
S9	33.50	1.53	4.96	1.79
S10	36.45	1.58	6.15	1.97
S11	38.55	2.29	10.10	2.10
S12	40.55	2.12	9.61	2.13
S13	47.50	0.81	3.68	2.14
S14	50.60	2.45	11.86	2.20
S15	64.40	0.26	1.36	2.27

σ_{dct} = DC conductivity in the transverse direction;
σ_{dcl} = DC conductivity in the longitudinal direction;
A_e = anisotropy coefficient

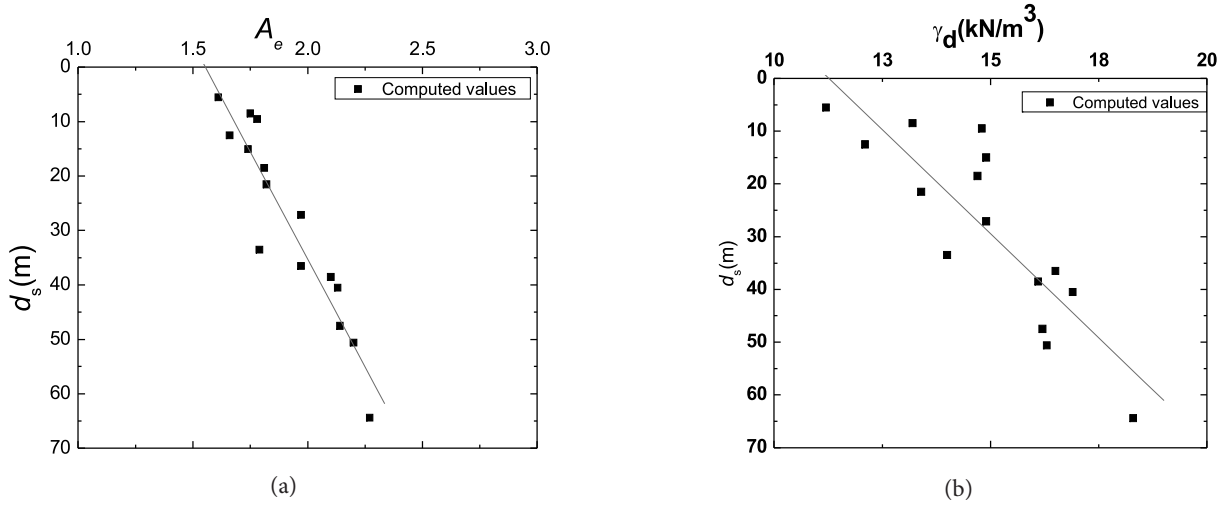

(a) (b)

Figure 3. Variation of (a) A_e and (b) γ_d with the depth of different samples.

this in view, A_e for different samples was computed (see Table 3) and its variation with respect to the sampling depth, d_s, is depicted in Fig. 3(a). Also, the variation of γ_d, with respect to d_s is depicted in Fig. 3(b).

It is clear from the trends depicted in Fig. 3 that with an increase in d_s, A_e and γ_d increase linearly. These trends can be attributed to the variation in the spatial arrangement of the soil particles and the pores, along the depth of the sediment deposition. This can be confirmed from Table 4, where the macro pores reduce nearly linearly with depth (i.e., from 42.04 % for S1, at 5.5 m depth, to 6.61% for S15, at 64.4 m depth).

Table 4. Summary of the MIP results for different samples.

Sample Designation	Macro-pores (%)	Meso-pores (%)	Micro-pores (%)	$^*d_d$ (μm)	$^*d_m$ (μm)
S1	42.04	52.59	5.37	0.04-0.3	0.043
S4	30.22	65.00	4.78	0.03-0.1	0.036
S7	23.43	68.84	7.73	0.02-0.06	0.029
S11	12.80	84.13	3.07	0.02-0.06	0.026
S14	9.55	84.73	5.72	0.008-0.02	0.023
S15	6.61	78.77	14.62	0.007-0.03	0.018

$^*d_d$ = Dominant pore diameter;
$^*d_m$ = Mean pore diameter

Furthermore, up to 15 m depth, comparatively smaller values of A_e (≈1.7) are observed. In this context, researchers [48] have reported that A_e for undisturbed samples is higher than that of the remoulded samples and undisturbed soil samples, with dispersed fabric structure, exhibit A_e≈2.0. It has also been stated by these researchers that the transition from the flocculated to the dispersed structure, for the remoulded samples, occurs at A_e≈1.6. Hence, A_e≈1.7 reflects a random arrangement, or a small degree of preferred orientation of the particles, in the natural soil deposits. This type of particle arrangement, referred to as a 'Flocculated' fabric, would normally be associated with comparatively younger sediments in the seabed. In this fabric, particles get attracted to one another in a very loose, haphazard manner, resulting in higher values of the voids ratio, *e*. However, a further decrease in *e*, with a corresponding increase in d_s, clearly indicates that sediments develop denser fabrics. This phenomenon can also be attributed to a subsequent increase in the overburden pressure, which the initial fabric would not be able to sustain as a result of the continuous accumulation of sediments. In other words, self-weight consolidation [2-6] would cause the rearrangement, or reorientation, of the particles in the preferred direction, progressively, which is reflected in an increase in A_e [≥2.0 for d_s>35 m, see Fig. 3(a)]. As such, higher values of A_e clearly indicate an increasing degree of preferred orientation of the particles in the horizontal plane. In other words, the fabric appears to be more anisotropic with the increase in depth, which is a typical characteristic of the dispersed fabric. Hence, it can be stated that with an increase in the depth of marine clays, the initially developed flocculated fabric is changed to a dispersed fabric and this alteration could be captured, quantitatively, in terms of A_e, relatively easily and quickly. In order to verify this hypothesis the results obtained from MIP and SEM were further analysed, as discussed in the following.

Samples S1, S4, S7, S11, S14 and S15 were analysed by employing the SEM and MIP techniques. Based on the data presented in Table 1, the samples used in the present study can be considered to represent sediments ranging from shallow depths (up to 35 m) to greater depths (>35 m). The SEM images of the specimens of these samples are depicted in Figures 4 to 8.

For instance, the SEM images of specimen S1 (taken in the horizontal plane of the sample, as depicted in Figure 4), which is a younger sediment than its counterparts, reveal that the fabric exhibits mainly 'edge-to-edge' and/or 'edge-to-face' contacts between the clay particles that are randomly orientated [23]. From the figure it can also be observed that it is a typical case of a honeycomb fabric [56] or a cellularity, by which sediments have been deposited in the form of continuous chains, as depicted in Fig. 4(a). This phenomenon can be attributed to the electrolyte-rich conditions of the marine environment, which is mainly due to the presence of a high chloride content. And due to this, the sediments are deposited in the form of flocs or agglomeration, and hence as a result a highly porous fabric is observed. Incidentally, Fig. 4(b) does not exhibit any sign of stratification (parallel orientation of clay platelets). Thus, it is a typical fabric of the marine clay that has been subjected to a negligible overburden pressure, due to the shallow depth of the deposition. On the other hand, for specimen S4 the SEM images are depicted in Figure 5. These micrographs reveal the presence of a typical matrix fabric [56], wherein larger gaps between the silt particles are found to be occupied by agglomerated clay platelets. From the results presented in Table 2, a comparatively higher percentage of silt fraction can be confirmed for sample S4. Such a type of fabric is relatively common among poorly and moderately consolidated marine clays (i.e., those deposited in an estuary), with a dry density not higher than 16.5 kN/m^3 [57].

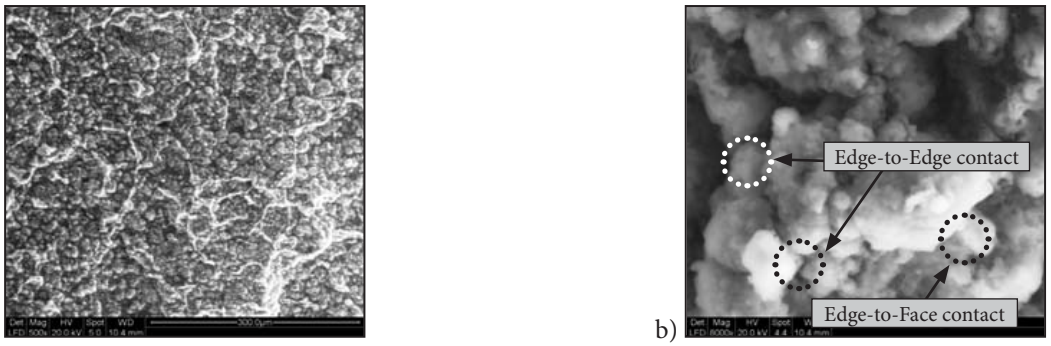

Figure 4. SEM images of S1 along horizontal (transverse) plane.

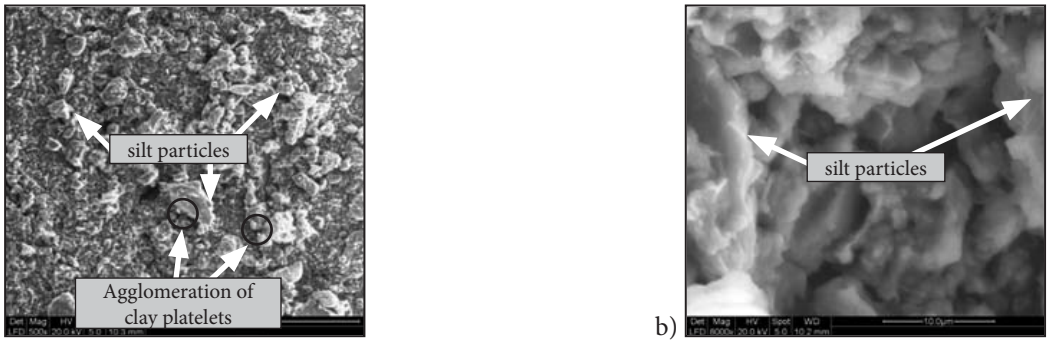

Figure 5. SEM images of S4 along horizontal (transverse) plane.

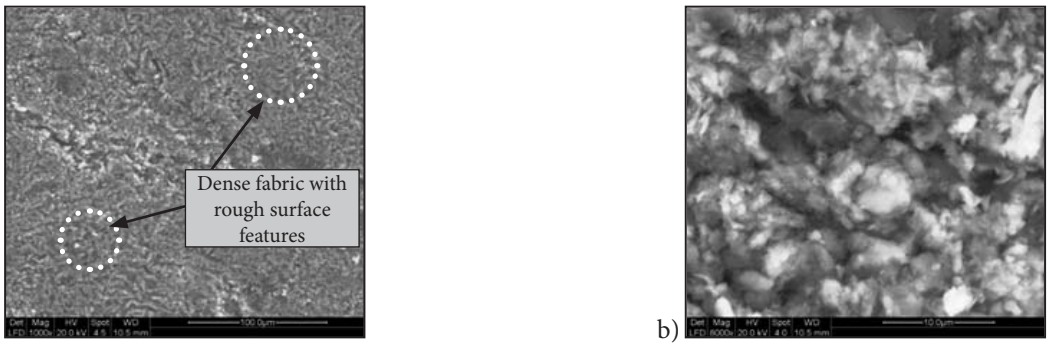

Figure 6. SEM images of S11 along horizontal (transverse) plane.

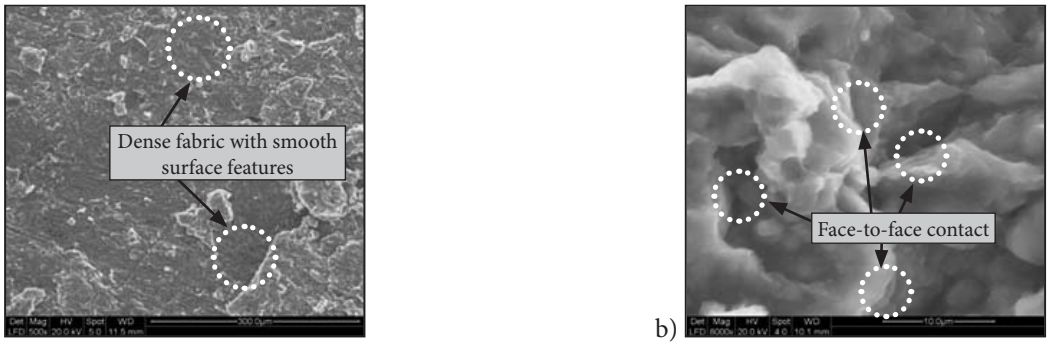

Figure 7. SEM images of S14 along horizontal (transverse) plane.

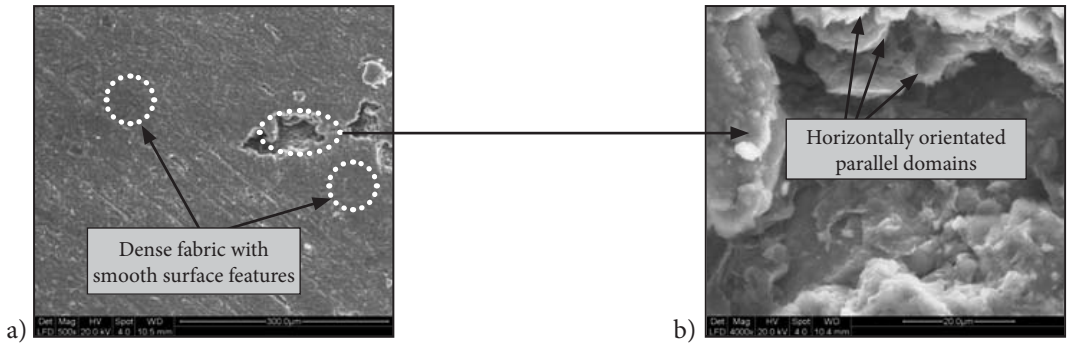

Figure 8. SEM images of S15 along horizontal (transverse) plane.

However, with a further increase in depth, the fabric acquires a dense structure with a specific orientation (face-to-face orientation) of particles with rough or smooth surface features and the presence of small pores), as depicted in Figures 6, 7 and 8, for the specimens S11, S14 and S15, respectively. This again can be attributed to the self-weight consolidation at deeper depths. Hence, the distinctive orientation of the clay platelets is observed to be in the transverse plane that is perpendicular to the direction of self-weight consolidation and which ultimately results in a 'face-to-face' contact between them [23]. These platelets increasingly become oriented parallel to each other, thereby making the fabric highly anisotropic. Thus, it can be concluded that with an increase in the depth, the particles and pores rearrange or reorient themselves into a new fabric that can be referred to as a 'dispersed' fabric.

In order to verify the above-mentioned findings, which are based on SEM, MIP studies were also conducted on the same specimens. The variation of the percentage cumulative volume of mercury intruded in the specimen, V_{Hg}, with respect to the pore diameter d was plotted as depicted in Fig. 9, from which the percentages of micro-pores (d<0.01μm), meso-pores (0.01μm<d<0.05μm) and macro-pores (0.05μm<d<10μm) present in the specimen [58] were determined. In addition, for each specimen, d_m which is the mean pore diameter and which corresponds to the pore diameter at which 50% of the pore volume gets intruded in the pore-size range considered [59], was also determined. The dominant pore diameter, d_d, which corresponds to the pore diameter at which the maximum incremental volume of mercury is intruded into the specimen (i.e., the maximum numbers of pores in the specimen are of this diameter), was determined as a diameter corresponding to the maximum (peak) incremental volume, V_{HgI}, in the plot between V_{HgI} and pore diameter [34]. However, it should be noted that multiple peaks were observed in the plot between

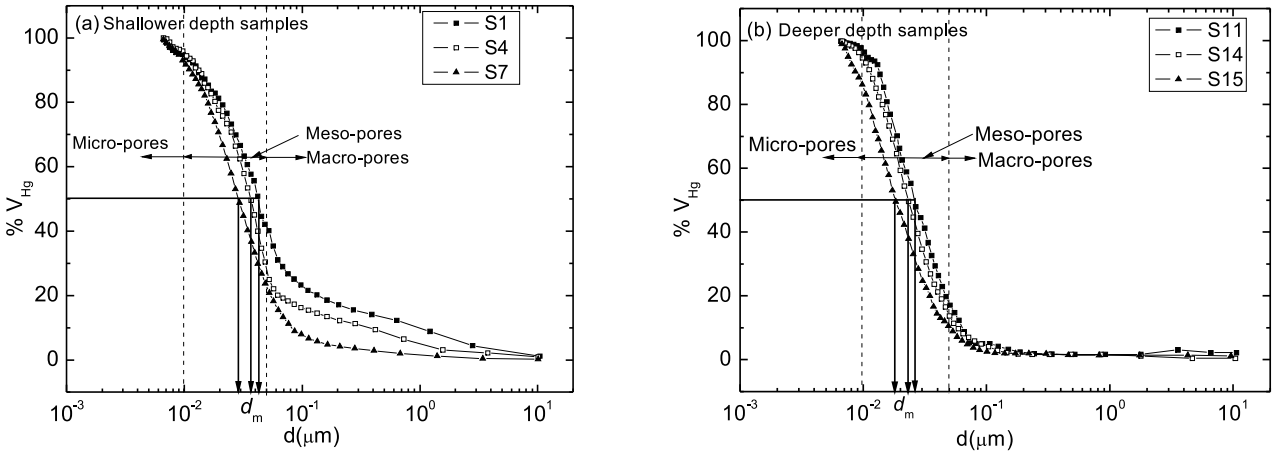

Figure 9. Pore size distribution w.r.t. % cumulative intrusion volume of mercury.

the V_{Hgl} and pore diameter, and hence the range of the dominant pore sizes can be defined as listed in Table 4. Furthermore, from the table it can be noted that as the depth increases, the percentage of macro-pores, and the value of d_m, decreases. In contrast, an increase in the percentages of meso- and micro-pores can be observed with an increase in the depth. For instance, specimens S1, S4 and S7 at lower depths exhibit a higher volume of macro pores (23.4 to 42 %) and a moderate volume of meso pores (52.6 to 68.6%), which represents a poorly-to-moderately consolidated deposit that exhibits a flocculated fabric structure. In contrast, specimens S11, S14 and S15 at higher depths exhibit a relatively lower volume of macro pores (6.6 to 12.8%) and a higher volume of meso pores (78.7 to 84.7%), representing a dense and highly consolidated deposit that exhibits a dispersed fabric structure. In other words, it can be said that with an increase in depth, the dominance of intra-aggregate pores, d<1.5 μm [34] over inter-aggregate pores, d≥1.5 μm, increases. This can be attributed to the reorganization and reorientation of clay platelets with an increase in depth (i.e., due to self-weight consolidation), which is responsible for the alteration of the randomly oriented fabric to the dispersed fabric. Hence, it can be inferred that the change in the fabric anisotropy, which in turn depends on alterations in the fabric structure, is related to a change in the size of the pores.

Furthermore, in order to highlight the importance of the study, the results obtained from the IS, SEM and MIP were superimposed in Fig. 10. It is clear from this figure, and Tables 1, 3 and 4, that the specimens S1, S4 and S7 exhibit a value of A_e between 1.61 and 1.82 and

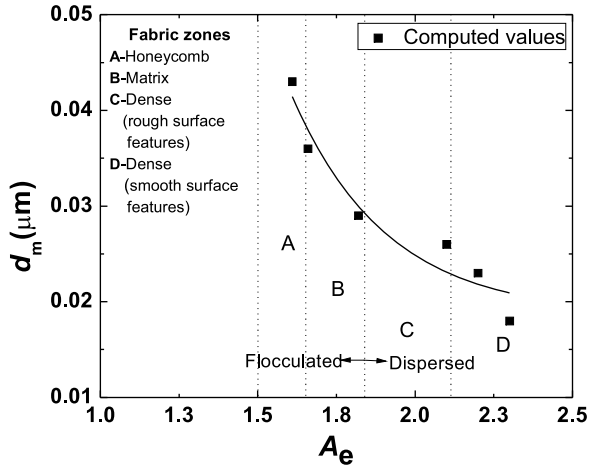

Figure 10. Variation in the fabric structure for Marine clay.

d_m values between 0.029 to 0.043 μm. The lower values of A_e and the relatively higher values of d_m indicate a honeycomb-type or matrix-type flocculated structure [60]. The analysis of the SEM images of these specimens (see Figs. 4 and 5), as described earlier, also qualitatively confirms the flocculated structure. In addition, it can be seen that for specimens S11, S14 and S15, A_e lies between 1.97 and 2.27 and the dm values are observed to be between 0.018 to 0.026 μm. Hence, it can be inferred that the higher A_e (≥ 2.0) and lower d_m would be representative of the dispersed structure. These fabric arrangements could be qualitatively observed in their SEM images (see Figs. 6 to 8). Hence, it can be hypothesized that Fig. 10 presents guidelines for determining the fabric (i.e., its type and the corresponding d_m) of the marine clays, if their A_e is known. It must be appreciated that a determination of A_e is relatively easy and less time consuming as compared to the SEM and MIP techniques. However, for a generalization of these findings, exhaustive investigations should be conducted on marine clays obtained from different locations and that too in the depth ranges beyond those covered in the present study.

Incidentally, it is worth mentioning here that the marine clay samples, which were retrieved from the offshore environment and transported to the laboratory, might have undergone changes from their undisturbed in-situ state due to various factors, such as sampling disturbance, relief of stresses from the sample during and after soil sampling, and smearing effects [61]. Also, the extraction of the sample from deeper locations would cause stress relaxation due to the removal of overburden and confining stresses and might result in a swelling of the samples [62, 63]. Furthermore, the soil below the drilled borehole might be subjected to higher vertical stresses, which might lead to localized compaction and disturbance of the soil layer beneath. Also, the mechanical disturbance caused by driving the sampler causes shear distortion and subsequent compression or remoulding of the soil (i.e., smearing) very close to the inner face of the sampler [63, 64]. These effects of stress relaxation, smearing and local disturbances could be different depending on the sampling depth and the overall characteristics of the soil (i.e., physical, chemical and mineralogical properties). The authors would like to reiterate that though the above mentioned factors might result in changes in the pore and fabric structure of the soils, which is responsible for changes in their anisotropy, the sampling procedure adopted in this study (i.e., the use of a sampler with an area ratio less than 10% for undisturbed soil sampling and careful extrusion of specimens for MIP, IS and SEM studies) ensures that these effects are minimal.

4 CONCLUDING REMARKS

In this study efforts were made to investigate the variation of the fabric of marine clays that were obtained from different depths below the seabed, in their undisturbed state. To achieve this, the anisotropy coefficient, A_e, was determined with the help of Impedance Spectroscopy and the same was found to vary from 1.5 to 2.25, for samples obtained from depths of 5 m to 65 m. This variation can be attributed to the self-weight consolidation, which alters the fabric of these samples and renders them increasingly anisotropic, with an increase in the depth. This hypothesis was substantiated by observing the scanning electron micrographs of some selected samples from different depths and by determining their pore size distribution characteristics with the help of Mercury Intrusion Porosimetery. It was demonstrated that with an increase in depth, the fabric alters from randomly oriented (or flocculated) to oriented in a preferred direction (or dispersed) and there is a reduction in the mean pore diameter (from 0.05 μm to 0.015 μm). As such, it can be stated that Impedance Spectroscopy is an effective tool to investigate (and quantify) the fabric of marine clays, easily and quickly.

REFERENCES

[1] Katagiri, M., Imai, G. (1994). A new in-laboratory method to make homogeneous clayey samples and their mechanical properties. Soils Found. 34, 2, 87-93.

[2] Imai, G. (1980). Settling behavior of clay suspension. Soils Found. 20, 2, 61-77.

[3] Been, K., Sills, G.C. (1981). Self-weight consolidation of soft soils: an experimental and theoretical study. Geotechnique 31, No. 4, pp. 519-535.

[4] Lee, K., Sills, G. C. (1981). The consolidation of a soil stratum, including self-weight effects and large strains. Int. J. Numer. Anal. Methods Geomech. 5, 4, 405-428.

[5] Toorman, E.A. (1996). Sedimentation and self-weight consolidation: general unifying theory. Geotechnique 46, 1, 101-113.

[6] Toorman, E.A. (1999). Sedimentation and self-weight consolidation: constitutive equations and numerical modeling. Geotechnique 49, 6, 709-726.

[7] Sridharan, A., Prakash, K. (2003). Self-weight consolidation: compressibility behavior of segregated and homogeneous fine-grained sediments. Marine Georesources and Geotechnology 21, 73-80.

[8] Bjerrum, L. (1973). Geotechnical problems involved in foundation of structures in North sea. Geotechnique 23, 3, 319-358.

[9] Bryant, W. R., Cernock, P., Morelock, J. (1967). Shear strength and consolidation characteristics of marine sediments from the western Gulf of Mexico. In: Richards, A.F. (Ed.), Marine Geotechnique. University of Illinois Press, Urbana, IL, 41-61.

[10] Richards, A.F. (Ed.), (1967). Marine Geotechnique, University of Illinois Press, Urbana, IL., 237.

[11] Gillot, J. E. (1968). Clay in Engineering Geology. Elsevier, London.

[12] Rashid, M.A., Brown, J.D. (1974). Influence of marine organic compounds on the engineering properties of a remoulded sediment. Engg. Geol. 9, 141-154.

[13] Katti, R.K. (1975). Regional soil deposits of India. Proceedings 5th Asian Regional Conf. on SM and FE, Bangalore, India, 11, 1-98.

[14] Penner, E., Burn, K.N. (1978). Review of engineering behavior of marine clays in eastern Canada. Can. Geotech. Journal 15, 2, 269-282.

[15] Egashira, K., Ohtsubo, M. (1982). Smectite in marine quick clays of Japan. Clays Clay Miner. 30, 4, 275-280.

[16] Torrance, J.K. (1975). On the role of chemistry in the development and behaviour of the sensitive marine clays of Canada and Scandinavia. Can. Geotech. Journal 12, 3, 326-335.

[17] Rajasekaran, G., Murali, K., Srinivasaraghavan, R. (1999). Microfabric, chemical and mineralogical study of Indian marine clays. Ocean Engineering, 26, 5, 463-483.

[18] Yanjun, D., Shenglin, L., Shigenori, H. (1999). Swelling-shrinkage properties and soil improvement of compacted expansive soil, Ning-Liang Highway, China. Engg. Geol. 53, 351-358.

[19] Lambe, T.W. (1958). The structure of compacted clay. Journal of the Soil Mechanics and Foundations Division, Proceedings of the American Society of Civil Engineers, Paper 1654 SM2, 1-34.

[20] Lafeber, D. (1962). Aspects, of stress-induced differential movements of fabric elements in mineral soils. Australian Road Research Board 1, 1059-1067.

[21] Ingles, O.G., Lafeber, D. (1966). The influence of volume defects on the strength and strength isotropy of stabilized clays. Engineering Geology 1, 305-310.

[22] Diamond, S. (1970). Pore Size Distribution in Clays. Clays Clay Miner. 18, 7-23.

[23] McConnachie, I. (1974). Fabric changes in consolidated Kaolin. Geotechnique 24, 207-222.

[24] Brewer, R. (1976). Fabric and Mineral Analysis of Soils. Robert E. Krieger Publishing, Huntinton, NY.
[25] Murphy, C.P., Bullock, P., Biswell, K.J. (1977). The measurement and characterization of voids in soil thin sections by image analysis: Part II. Applications. Journal of Soil Science 28, 509-518.
[26] Collins, K. (1983). Scanning electron microscopy of engineering soils. Geoderma 30, 1-4, 243-252.
[27] Delage, P., Lefebvre, G. (1984). Study of the structure of a sensitive Champlain clay and its evolution during consolidation. Can. Geotech, J. 21, 1, 21-35.
[28] Griffiths, F.J., Joshi, R.C. (1989). Change in pore size distribution due to consolidation of clays. Geotechnique 39, 1, 159-167.
[29] Mitchell, J.K. (1993). Fundamentals of Soil Behavior, John Wiley & Sons, New York.
[30] Basma, A. ., Azm, S. A., Malkawi, A.I.H., Mohamed, A.A.B. (1996). Swelling-shrinkage behavior of natural expansive clays. App. Clay Sci. 11, 2-4, 211-227.
[31] Rao, S.M., Revanasiddappa, K. (2005). Role of microfabric in matrix suction of residual soils. Engng. Geol. 80, 1-2, 60-70.
[32] Dolinar, B., Trauner, L. (2007). The impact of structure on the undrained shear strength of cohesive soils, Engng. Geol. 92, 1-2, 88-96.
[33] Wang, Y.H., Xu, D. (2007). Dual Porosity and Secondary Consolidation. J. Geotech. Geoenviron. Engng., ASCE, 133, 7, 793-801.
[34] Souli, H., Fleureau, M., Trabelsi Ayadi, M., Besnard, M. (2008). Physicochemical analysis of permeability changes in the presence of zinc. Geoderma 145, 1-2, 1-7.
[35] Yong, R. N., and Warkentin, B. P. (1966). Introduction to Soil Behaviour. MacMillan, New York.
[36] Ospiv, V.I. (1983). Methods of studying clay microstructure. Geotech. Test. J. ASTM 6, 1, 10-17.
[37] McManis, J., Ferrel, R.E.Jr., Arman, A. (1983). Interpreting the physical properties of a clay using microanalysis technique. Geotech. Test. J., ASTM 6, 2, 87-92.
[38] Tovey, N.K. (1975). A mineralogical and microfabric study of Chek Lap Kok marine clay. Research Report No. Rr.3/85, Geotech. Control Office, Hong Kong, 138.
[39] Tovey, N.K. (1986). Microfabric, chemical and mineralogical studies of soils: techniques. J. Geotech. Engng, ASCE 17, 131-166.
[40] Jones, M. (1994). Mechanical principles of sediment deformation. In: Maltman, A. (Ed.), The Geological Deformation of Sediment. Chapman and Hall, London, 37-71.
[41] ASTM D 5550 (2000). Standard test method for specific gravity of soil solids by gas pycnometer. Annual Book of ASTM Standards 04.08, ASTM International, West Conshohocken, PA, USA.
[42] Kulkarni, M.P., Patel, A., Singh, D.N. (2010). Application of shear wave velocity for characterizing clays from coastal regions. J. Civil Eng. KSCE. 3, 14, 307-321.
[43] ASTM D 422-63 (1994). Standard test method for particle size analysis of soils. Annual Book of ASTM Standards 04.08, ASTM International, West Conshohocken, PA, USA.
[44] ASTM D 4318-93 (1994). Standard test methods for liquid limit, plastic limit, and plasticity index of soils. Annual Book of ASTM Standards 04.08, ASTM International, West Conshohocken, PA, USA.
[45] ASTM D 2487-06e1, (2006). Standard practice for classification of soils for engineering purposes (Unified Soil Classification System). Annual Book of ASTM Standards 04.18, ASTM International, West Conshohocken, PA, USA.
[46] Mousseau , R.J., and Trump, R. (1967). Measurement of electrical anisotropy of clay-like materials. Journal of Applied Physics 38, 11, 4375-4379.
[47] McCarter, W.J., Blewett, J., Chrisp, T.M., Starrs, G. (2005). Electrical property measurements using a modified hydraulic oedometer. Can. Geotech. Journal 42, 2, 655-662.
[48] Gumaste, S.D., Singh, D.N. (2010). Application of impedance spectroscopy for determining fabric anisotropy of fine grained soils. J. Test. Eval., ASTM 38, 3, 309-319.
[49] Arulanandan, K., Smith, S.S. (1973). Electrical dispersion in relation to soil structure. J. Soil Mech. Foundation Engineering, ASCE 99, 1113-1133.
[50] McCarter, W.J., Desmazes, P. (1997). Soil Characterization Using Electrical Measurements. Geotechnique 47, 1, 179-183.
[51] Rinaldi, V.A., Francisca, F.M. (1999). Impedance analysis of soil dielectric dispersion (1 MHz–1GHz), J. Geotech. Geoenviron. Eng., ASCE 125, 2, 111-121.
[52] Shah, P.H., Singh, D.N. (2004). A Simple Methodology for Determining Electrical Conductivity of Soils. J. ASTM Int. 1, 5, 1-11.
[53] Leon, A.C. (1998). New perspectives in mercury porosimetry, Advances in Colloid and Interface Science 76-77, 341-372.
[54] Guidi, G., Poggio, G., Petruzzell, G. (1985). The porosity of soil aggregates from bulk soil and from soil adhering to roots. Plant and Soil 87, 311-314.
[55] Anandrajah, A., Kuganenthira, N., and Zhao, D. (1996). Variation of fabric anisotropy of kaolinite

in triaxial loading. J. Geotech. Engg., ASCE 122, 8, 633-640.
[56] Collins, K., McGown, A. (1974). The form and function of microfabric features in a variety of natural soils. Geotechnique 24, 2, 223-254.
[57] Gorokhova, I.M. (1966). Theoretical fundaments for the evaluation of sedimentary rocks for engineering geological purposes. Nauka Publ., Moscow.
[58] Moon, H. Y., Kim, H. S., Choi, D. S. (2006). Relationship between Average Pore diameter and chloride diffusivity in various concretes. Const. Build. Mater. 20, 725-732.
[59] Li, S., Roy, D.M. (1986). Investigation of relations between porosity, pore structure, and C1– diffusion of fly ash and blended cement pastes. Cement Concrete Research 16, 5, 749-759.
[60] Gumaste, S. (2010). Determination of fabric of fine-grained soils, PhD thesis submitted to Civil Engineering Department, IIT Bombay.
[61] Blomqvist, S. (1991). Quantitative sampling of soft-bottom sediments: problems and solutions. Marine Ecology Progress Series 72, 295-304.
[62] Hvorslev, M.J. (1949). Subsurface exploration and sampling of soils for civil engineering purposes. U. S. Army Corps of Engineers, Waterways Experimental Station, Vicksburg, Mississippi.
[63] Bashar, M.A., Siddique, A., Safiullah, A.M.M. (1997). Effect of stress relief disturbance on undrained shear properties of Chittagong coastal soils. Journal of Civil Engineering, The Institution of Engineers, Bangladesh 25, 1, 65-77.
[64] Schjetne, K. (1971). The measurement of pore pressure during sampling. Proc. Speciality on Quality in Soil Sampling, 4th Asian Conference, ICSMFE, Bangkok, 12-16.